Angular Analysis of $B^0 \to K^*(892)^0 \ell^+ \ell^-$

A. Abdesselam,[88] I. Adachi,[20,16] K. Adamczyk,[64] H. Aihara,[96] S. Al Said,[88,40] K. Arinstein,[5,68] Y. Arita,[57] D. M. Asner,[71] T. Aso,[101] H. Atmacan,[53] V. Aulchenko,[5,68] T. Aushev,[56] R. Ayad,[88] T. Aziz,[89] V. Babu,[89] I. Badhrees,[88,39] S. Bahinipati,[25] A. M. Bakich,[87] A. Bala,[72] Y. Ban,[73] V. Bansal,[71] E. Barberio,[52] M. Barrett,[19] W. Bartel,[10] A. Bay,[45] I. Bedny,[5,68] P. Behera,[27] M. Belhorn,[9] K. Belous,[31] D. Besson,[55] V. Bhardwaj,[24] B. Bhuyan,[26] J. Biswal,[34] T. Bloomfield,[52] S. Blyth,[62] A. Bobrov,[5,68] A. Bondar,[5,68] G. Bonvicini,[104] C. Bookwalter,[71] C. Boulahouache,[88] A. Bozek,[64] M. Bračko,[50,34] F. Breibeck,[30] J. Brodzicka,[64] T. E. Browder,[19] E. Waheed,[52] D. Červenkov,[6] M.-C. Chang,[12] P. Chang,[63] Y. Chao,[63] V. Chekelian,[51] A. Chen,[61] K.-F. Chen,[63] P. Chen,[63] B. G. Cheon,[18] K. Chilikin,[46,55] R. Chistov,[46,55] K. Cho,[41] V. Chobanova,[51] S.-K. Choi,[17] Y. Choi,[86] D. Cinabro,[104] J. Crnkovic,[23] J. Dalseno,[51,90] M. Danilov,[55,46] N. Dash,[25] S. Di Carlo,[104] J. Dingfelder,[4] Z. Doležal,[6] Z. Drásal,[6] A. Drutskoy,[46,55] S. Dubey,[19] D. Dutta,[89] K. Dutta,[26] S. Eidelman,[5,68] D. Epifanov,[96] S. Esen,[9] H. Farhat,[104] J. E. Fast,[71] M. Feindt,[36] T. Ferber,[10] A. Frey,[15] O. Frost,[10] B. G. Fulsom,[71] V. Gaur,[89] N. Gabyshev,[5,68] S. Ganguly,[104] A. Garmash,[5,68] D. Getzkow,[13] R. Gillard,[104] F. Giordano,[23] R. Glattauer,[30] Y. M. Goh,[18] P. Goldenzweig,[36] B. Golob,[47,34] D. Greenwald,[91] M. Grosse Perdekamp,[23,78] J. Grygier,[36] O. Grzymkowska,[64] H. Guo,[80] J. Haba,[20,16] P. Hamer,[15] Y. L. Han,[29] K. Hara,[20] T. Hara,[20,16] Y. Hasegawa,[82] J. Hasenbusch,[4] K. Hayasaka,[66] H. Hayashii,[60] X. H. He,[73] M. Heck,[36] M. T. Hedges,[19] D. Heffernan,[70] M. Heider,[36] A. Heller,[36] T. Higuchi,[37] S. Himori,[94] S. Hirose,[57] T. Horiguchi,[94] Y. Hoshi,[93] K. Hoshina,[99] W.-S. Hou,[63] Y. B. Hsiung,[63] C.-L. Hsu,[52] M. Huschle,[36] H. J. Hyun,[44] Y. Igarashi,[20] T. Iijima,[58,57] M. Imamura,[57] K. Inami,[57] G. Inguglia,[10] A. Ishikawa,[94] K. Itagaki,[94] R. Itoh,[20,16] M. Iwabuchi,[106] M. Iwasaki,[96] Y. Iwasaki,[20] S. Iwata,[98] W. W. Jacobs,[28] I. Jaegle,[19] H. B. Jeon,[44] D. Joffe,[38] M. Jones,[19] K. K. Joo,[8] T. Julius,[52] H. Kakuno,[98] J. H. Kang,[106] K. H. Kang,[44] P. Kapusta,[64] S. U. Kataoka,[59] E. Kato,[94] Y. Kato,[57] P. Katrenko,[56,46] H. Kawai,[7] T. Kawasaki,[66] T. Keck,[36] H. Kichimi,[20] C. Kiesling,[51] B. H. Kim,[81] D. Y. Kim,[84] H. J. Kim,[44] H.-J. Kim,[106] J. B. Kim,[42] J. H. Kim,[41] K. T. Kim,[42] M. J. Kim,[44] S. H. Kim,[18] S. K. Kim,[81] Y. J. Kim,[41] K. Kinoshita,[9] C. Kleinwort,[10] J. Klucar,[34] B. R. Ko,[42] N. Kobayashi,[97] S. Koblitz,[51] P. Kodyš,[6] Y. Koga,[57] S. Korpar,[50,34] D. Kotchetkov,[19] R. T. Kouzes,[71] P. Križan,[47,34] P. Krokovny,[5,68] B. Kronenbitter,[36] T. Kuhr,[48] R. Kumar,[75] T. Kumita,[98] E. Kurihara,[7] Y. Kuroki,[70] A. Kuzmin,[5,68] P. Kvasnička,[6] Y.-J. Kwon,[106] Y.-T. Lai,[63] J. S. Lange,[13] D. H. Lee,[42] I. S. Lee,[18] S.-H. Lee,[42] M. Leitgab,[23,78] R. Leitner,[6] D. Levit,[91] P. Lewis,[19] C. H. Li,[52] H. Li,[28] J. Li,[81] L. Li,[80] X. Li,[81] Y. Li,[103] L. Li Gioi,[51] J. Libby,[27] A. Limosani,[52] C. Liu,[80] Y. Liu,[9] Z. Q. Liu,[29] D. Liventsev,[103,20] A. Loos,[85] R. Louvot,[45] M. Lubej,[34] P. Lukin,[5,68] T. Luo,[74] J. MacNaughton,[20] M. Masuda,[95] T. Matsuda,[54] D. Matvienko,[5,68] A. Matyja,[64] S. McOnie,[87] Y. Mikami,[94] K. Miyabayashi,[60] Y. Miyachi,[105] H. Miyake,[20,16] H. Miyata,[66] Y. Miyazaki,[57] R. Mizuk,[46,55,56] G. B. Mohanty,[89] S. Mohanty,[89,102] D. Mohapatra,[71] A. Moll,[51,90] H. K. Moon,[42] T. Mori,[57] T. Morii,[37] H.-G. Moser,[51] T. Müller,[36] N. Muramatsu,[76] R. Mussa,[33] T. Nagamine,[94] Y. Nagasaka,[21] Y. Nakahama,[96] I. Nakamura,[20,16] K. R. Nakamura,[20] E. Nakano,[69] H. Nakano,[94] T. Nakano,[77] M. Nakao,[20,16] H. Nakayama,[20,16] H. Nakazawa,[61] T. Nanut,[34] K. J. Nath,[26] Z. Natkaniec,[64] M. Nayak,[104] E. Nedelkovska,[51] K. Negishi,[94] K. Neichi,[93] C. Ng,[96] C. Niebuhr,[10] M. Niiyama,[43] N. K. Nisar,[89,1] S. Nishida,[20,16] K. Nishimura,[19] O. Nitoh,[99] T. Nozaki,[20] A. Ogawa,[78] S. Ogawa,[92] T. Ohshima,[57] S. Okuno,[35] S. L. Olsen,[81] Y. Ono,[94] Y. Onuki,[96] W. Ostrowicz,[64] C. Oswald,[4] H. Ozaki,[20,16] P. Pakhlov,[46,55] G. Pakhlova,[46,56] B. Pal,[9] H. Palka,[64] E. Panzenböck,[15,60] C.-S. Park,[106] C. W. Park,[86] H. Park,[44] K. S. Park,[86] S. Paul,[91] L. S. Peak,[87] T. K. Pedlar,[49] T. Peng,[80] L. Pesántez,[4] R. Pestotnik,[34] M. Peters,[19] M. Petrič,[34] L. E. Piilonen,[103] A. Poluektov,[5,68] K. Prasanth,[27] M. Prim,[36] K. Prothmann,[51,90] C. Pulvermacher,[36] M. V. Purohit,[85] J. Rauch,[91] B. Reisert,[51] E. Ribežl,[34] M. Ritter,[48] M. Röhrken,[36] J. Rorie,[19] A. Rostomyan,[10] M. Rozanska,[64] S. Rummel,[48] S. Ryu,[81] H. Sahoo,[19] T. Saito,[94] K. Sakai,[20] Y. Sakai,[20,16] S. Sandilya,[9] D. Santel,[9] L. Santelj,[20] T. Sanuki,[94] N. Sasao,[43] Y. Sato,[57] V. Savinov,[74] T. Schlüter,[48] O. Schneider,[45] G. Schnell,[2,22] P. Schönmeier,[94] M. Schram,[71] C. Schwanda,[30] A. J. Schwartz,[9] B. Schwenker,[15] R. Seidl,[78] Y. Seino,[66] D. Semmler,[13] K. Senyo,[105] O. Seon,[57] I. S. Seong,[19] M. E. Sevior,[52] L. Shang,[29] M. Shapkin,[31] V. Shebalin,[5,68] C. P. Shen,[3] T.-A. Shibata,[97] H. Shibuya,[92] S. Shinomiya,[70] J.-G. Shiu,[63] B. Shwartz,[5,68] A. Sibidanov,[87] F. Simon,[51,90] J. B. Singh,[72] R. Sinha,[32] P. Smerkol,[34] Y.-S. Sohn,[106] A. Sokolov,[31] Y. Soloviev,[10] E. Solovieva,[46,56] S. Stanič,[67] M. Starič,[34] M. Steder,[10] J. F. Strube,[71] J. Stypula,[64] S. Sugihara,[96] A. Sugiyama,[79] M. Sumihama,[14] K. Sumisawa,[20,16] T. Sumiyoshi,[98] K. Suzuki,[57] S. Suzuki,[79] S. Y. Suzuki,[20] Z. Suzuki,[94] H. Takeichi,[57] M. Takizawa,[83] U. Tamponi,[33,100] M. Tanaka,[20,16] S. Tanaka,[20,16] K. Tanida,[81] N. Taniguchi,[20] G. N. Taylor,[52]

arXiv:1604.04042v2 [hep-ex] 16 Apr 2016

F. Tenchini,[52] Y. Teramoto,[69] I. Tikhomirov,[55] K. Trabelsi,[20,16] V. Trusov,[36] Y. F. Tse,[52] T. Tsuboyama,[20,16] M. Uchida,[97] T. Uchida,[20] S. Uehara,[20,16] K. Ueno,[63] T. Uglov,[46,56] Y. Unno,[18] S. Uno,[20,16] S. Uozumi,[44] P. Urquijo,[52] Y. Ushiroda,[20,16] Y. Usov,[5,68] S. E. Vahsen,[19] C. Van Hulse,[2] P. Vanhoefer,[51] G. Varner,[19] K. E. Varvell,[87] K. Vervink,[45] A. Vinokurova,[5,68] V. Vorobyev,[5,68] A. Vossen,[28] M. N. Wagner,[13] E. Waheed,[52] C. H. Wang,[62] J. Wang,[73] M.-Z. Wang,[63] P. Wang,[29] X. L. Wang,[103] M. Watanabe,[66] Y. Watanabe,[35] R. Wedd,[52] S. Wehle,[10] E. White,[9] J. Wiechczynski,[64] K. M. Williams,[103] E. Won,[42] B. D. Yabsley,[87] S. Yamada,[20] H. Yamamoto,[94] J. Yamaoka,[71] Y. Yamashita,[65] M. Yamauchi,[20,16] S. Yashchenko,[10] H. Ye,[10] J. Yelton,[11] Y. Yook,[106] C. Z. Yuan,[29] Y. Yusa,[66] C. C. Zhang,[29] L. M. Zhang,[80] Z. P. Zhang,[80] L. Zhao,[80] V. Zhilich,[5,68] V. Zhukova,[55] V. Zhulanov,[5,68] M. Ziegler,[36] T. Zivko,[34] A. Zupanc,[47,34] N. Zwahlen,[45] and O. Zyukova[5,68]

(The Belle Collaboration)

[1]*Aligarh Muslim University, Aligarh 202002*
[2]*University of the Basque Country UPV/EHU, 48080 Bilbao*
[3]*Beihang University, Beijing 100191*
[4]*University of Bonn, 53115 Bonn*
[5]*Budker Institute of Nuclear Physics SB RAS, Novosibirsk 630090*
[6]*Faculty of Mathematics and Physics, Charles University, 121 16 Prague*
[7]*Chiba University, Chiba 263-8522*
[8]*Chonnam National University, Kwangju 660-701*
[9]*University of Cincinnati, Cincinnati, Ohio 45221*
[10]*Deutsches Elektronen–Synchrotron, 22607 Hamburg*
[11]*University of Florida, Gainesville, Florida 32611*
[12]*Department of Physics, Fu Jen Catholic University, Taipei 24205*
[13]*Justus-Liebig-Universität Gießen, 35392 Gießen*
[14]*Gifu University, Gifu 501-1193*
[15]*II. Physikalisches Institut, Georg-August-Universität Göttingen, 37073 Göttingen*
[16]*SOKENDAI (The Graduate University for Advanced Studies), Hayama 240-0193*
[17]*Gyeongsang National University, Chinju 660-701*
[18]*Hanyang University, Seoul 133-791*
[19]*University of Hawaii, Honolulu, Hawaii 96822*
[20]*High Energy Accelerator Research Organization (KEK), Tsukuba 305-0801*
[21]*Hiroshima Institute of Technology, Hiroshima 731-5193*
[22]*IKERBASQUE, Basque Foundation for Science, 48013 Bilbao*
[23]*University of Illinois at Urbana-Champaign, Urbana, Illinois 61801*
[24]*Indian Institute of Science Education and Research Mohali, SAS Nagar, 140306*
[25]*Indian Institute of Technology Bhubaneswar, Satya Nagar 751007*
[26]*Indian Institute of Technology Guwahati, Assam 781039*
[27]*Indian Institute of Technology Madras, Chennai 600036*
[28]*Indiana University, Bloomington, Indiana 47408*
[29]*Institute of High Energy Physics, Chinese Academy of Sciences, Beijing 100049*
[30]*Institute of High Energy Physics, Vienna 1050*
[31]*Institute for High Energy Physics, Protvino 142281*
[32]*Institute of Mathematical Sciences, Chennai 600113*
[33]*INFN - Sezione di Torino, 10125 Torino*
[34]*J. Stefan Institute, 1000 Ljubljana*
[35]*Kanagawa University, Yokohama 221-8686*
[36]*Institut für Experimentelle Kernphysik, Karlsruher Institut für Technologie, 76131 Karlsruhe*
[37]*Kavli Institute for the Physics and Mathematics of the Universe (WPI), University of Tokyo, Kashiwa 277-8583*
[38]*Kennesaw State University, Kennesaw, Georgia 30144*
[39]*King Abdulaziz City for Science and Technology, Riyadh 11442*
[40]*Department of Physics, Faculty of Science, King Abdulaziz University, Jeddah 21589*
[41]*Korea Institute of Science and Technology Information, Daejeon 305-806*
[42]*Korea University, Seoul 136-713*
[43]*Kyoto University, Kyoto 606-8502*
[44]*Kyungpook National University, Daegu 702-701*
[45]*École Polytechnique Fédérale de Lausanne (EPFL), Lausanne 1015*
[46]*P.N. Lebedev Physical Institute of the Russian Academy of Sciences, Moscow 119991*
[47]*Faculty of Mathematics and Physics, University of Ljubljana, 1000 Ljubljana*
[48]*Ludwig Maximilians University, 80539 Munich*
[49]*Luther College, Decorah, Iowa 52101*
[50]*University of Maribor, 2000 Maribor*
[51]*Max-Planck-Institut für Physik, 80805 München*

[52] School of Physics, University of Melbourne, Victoria 3010
[53] Middle East Technical University, 06531 Ankara
[54] University of Miyazaki, Miyazaki 889-2192
[55] Moscow Physical Engineering Institute, Moscow 115409
[56] Moscow Institute of Physics and Technology, Moscow Region 141700
[57] Graduate School of Science, Nagoya University, Nagoya 464-8602
[58] Kobayashi-Maskawa Institute, Nagoya University, Nagoya 464-8602
[59] Nara University of Education, Nara 630-8528
[60] Nara Women's University, Nara 630-8506
[61] National Central University, Chung-li 32054
[62] National United University, Miao Li 36003
[63] Department of Physics, National Taiwan University, Taipei 10617
[64] H. Niewodniczanski Institute of Nuclear Physics, Krakow 31-342
[65] Nippon Dental University, Niigata 951-8580
[66] Niigata University, Niigata 950-2181
[67] University of Nova Gorica, 5000 Nova Gorica
[68] Novosibirsk State University, Novosibirsk 630090
[69] Osaka City University, Osaka 558-8585
[70] Osaka University, Osaka 565-0871
[71] Pacific Northwest National Laboratory, Richland, Washington 99352
[72] Panjab University, Chandigarh 160014
[73] Peking University, Beijing 100871
[74] University of Pittsburgh, Pittsburgh, Pennsylvania 15260
[75] Punjab Agricultural University, Ludhiana 141004
[76] Research Center for Electron Photon Science, Tohoku University, Sendai 980-8578
[77] Research Center for Nuclear Physics, Osaka University, Osaka 567-0047
[78] RIKEN BNL Research Center, Upton, New York 11973
[79] Saga University, Saga 840-8502
[80] University of Science and Technology of China, Hefei 230026
[81] Seoul National University, Seoul 151-742
[82] Shinshu University, Nagano 390-8621
[83] Showa Pharmaceutical University, Tokyo 194-8543
[84] Soongsil University, Seoul 156-743
[85] University of South Carolina, Columbia, South Carolina 29208
[86] Sungkyunkwan University, Suwon 440-746
[87] School of Physics, University of Sydney, New South Wales 2006
[88] Department of Physics, Faculty of Science, University of Tabuk, Tabuk 71451
[89] Tata Institute of Fundamental Research, Mumbai 400005
[90] Excellence Cluster Universe, Technische Universität München, 85748 Garching
[91] Department of Physics, Technische Universität München, 85748 Garching
[92] Toho University, Funabashi 274-8510
[93] Tohoku Gakuin University, Tagajo 985-8537
[94] Department of Physics, Tohoku University, Sendai 980-8578
[95] Earthquake Research Institute, University of Tokyo, Tokyo 113-0032
[96] Department of Physics, University of Tokyo, Tokyo 113-0033
[97] Tokyo Institute of Technology, Tokyo 152-8550
[98] Tokyo Metropolitan University, Tokyo 192-0397
[99] Tokyo University of Agriculture and Technology, Tokyo 184-8588
[100] University of Torino, 10124 Torino
[101] Toyama National College of Maritime Technology, Toyama 933-0293
[102] Utkal University, Bhubaneswar 751004
[103] Virginia Polytechnic Institute and State University, Blacksburg, Virginia 24061
[104] Wayne State University, Detroit, Michigan 48202
[105] Yamagata University, Yamagata 990-8560
[106] Yonsei University, Seoul 120-749

We present a measurement of angular observables, P_4', P_5', P_6', P_8', in the decay $B^0 \to K^*(892)^0\ell^+\ell^-$, where $\ell^+\ell^-$ is either e^+e^- or $\mu^+\mu^-$. The analysis is performed on a data sample corresponding to an integrated luminosity of 711 fb^{-1} containing 772×10^6 $B\bar{B}$ pairs, collected at the $\Upsilon(4S)$ resonance with the Belle detector at the asymmetric-energy e^+e^- collider KEKB. Four angular observables, $P'_{4,5,6,8}$ are extracted in five bins of the invariant mass squared of the lepton system, q^2. We compare our results for $P'_{4,5,6,8}$ with Standard Model predictions including the q^2 region in which the LHCb collaboration reported the so-called P_5' anomaly.

I. INTRODUCTION

Rare decays of B mesons are an ideal probe to search beyond the Standard Model (SM) of particle physics, since contributions from new particles lead to effects that are of similar size as the SM predictions. The rare decay $B^0 \to K^*(892)^0\ell^+\ell^-$involves the quark transition $b \to s\ell^+\ell^-$, a flavor changing neutral current that is forbidden at tree level in the SM. Higher order SM processes such as penguin or W^+W^- box diagrams allow for such transitions, leading to branching fractions of less than one in a million. Various extensions to the SM predict contributions from new physics, which can interfere with the SM amplitudes and lead to enhanced or suppressed branching fractions or modified angular distributions of the decay products.

We present an angular analysis, using the decay modes $B^0 \to K^*(892)^0\mu^+\mu^-$ and $B^0 \to K^*(892)^0e^+e^-$, in a data sample recorded with the Belle detector. The LHCb collaboration reported a discrepancy in the angular distribution of the decay $B^0 \to K^*(892)^0\mu^+\mu^-$, corresponding to a 3.4σ deviation from the SM prediction [1]. In contrast to the LHCb measurement here the di-electron channel is also used in this analysis.

II. DETECTOR AND DATASETS

We use the full $\Upsilon(4S)$ data sample containing 772×10^6 $B\bar{B}$ pairs recorded with the Belle detector [2] at the asymmetric-energy e^+e^- collider KEKB [3].

The Belle detector is a large-solid-angle magnetic spectrometer that consists of a silicon vertex detector (SVD), a 50-layer central drift chamber (CDC), an array of aerogel threshold Cherenkov counters (ACC), a barrel-like arrangement of time-of-flight scintillation counters (TOF), and an electromagnetic calorimeter comprised of CsI(Tl) crystals (ECL) located inside a super-conducting solenoid coil that provides a 1.5 T magnetic field. An iron flux-return located outside of the coil is instrumented to detect K_L^0 mesons and to identify muons (KLM). The detector is described in detail elsewhere [2].

This analysis is validated and optimized on simulated Monte Carlo (MC) data. The software packages EvtGen [4] and PYTHIA [5] are used to simulate the particle decays. The decay chain is generated, meaning that all intermediate and final state particles are determined. Final state radiation is calculated by the PHOTOS package [6]. The detector response is simulated with the GEANT3 software package [7].

III. RECONSTRUCTION

For all charged tracks loose impact parameter constraints are applied with respect to the nominal interaction point in the radial direction ($|dr| < 1.0$ cm) and along the beam direction ($|dz| < 5.0$ cm). Belle provides a particle identification (PID) likelihood calculated from the energy loss in the CDC ($\mathrm{d}E/\mathrm{d}x$), time-of-flight, response of ACC, shape and size of the showers in the ECL and information about hits in the KLM. Electrons are identified using the likelihood ratio $\mathcal{P}_{\rm eid}(e) = L(e)/(L(e) + L(\text{hadron}))$. All charged tracks satisfying $\mathcal{P}_{\rm eid}(e) > 0.1$ are accepted as electrons. To recover the original momentum of the electrons, a search for photons in a cone of 0.05 radians around the initial momentum direction of the track is performed. If photons are found in this region, their momenta are added to the electron. Charged tracks are accepted as muons if they satisfy the muon likelihood ratio requirement $\mathcal{P}_{\rm muid}(\mu) > 0.1$. Charged kaons are selected with the requirement on the likelihood $\mathcal{P}(K/\pi) = L(K)/(L(K) + L(\pi)) > 0.1$. For $\pi^\pm$ candidates no PID selection is applied.

K^* candidates are formed in the channel $K^{*0} \to K^+\pi^-$. For these candidates, an invariant mass requirement of $0.6\ \text{GeV}/c^2 < M_{K^*} < 1.4\ \text{GeV}/c^2$ is applied and a vertex fit is performed, which is used for background suppression later on.

In the final stage of the reconstruction K^* candidates are combined with oppositely charged lepton pairs to form B meson candidates. The large combinatoric background is suppressed by applying requirements on kinematic variables. Two independent variables can be constructed using constraints that in $\Upsilon(4S)$ decays B mesons are produced pairwise and each carries half the center–of–mass (CM) frame beam energy, $E_{\rm Beam}$. These variables are the beam constrained mass, $M_{\rm bc}$, and the energy difference, ΔE, in which signal features a distinct distribution that can discriminate against background. The variables are defined in the $\Upsilon(4S)$ rest frame as

$$M_{\rm bc} \equiv \sqrt{E_{\rm Beam}^2/c^4 - |\vec{p}_B|^2/c^2} \text{ and} \quad (1)$$

$$\Delta E \equiv E_B - E_{\rm Beam}, \quad (2)$$

where E_B and $|\vec{p}_B|$ are the energy and momentum of the reconstructed candidate, respectively. Correctly reconstructed candidates are located around the nominal B mass in $M_{\rm bc}$ and feature ΔE of around zero. Candidates are selected satisfying $5.22 < M_{\rm bc} < 5.3\ \text{GeV}/c^2$ and $-0.10\ (-0.05) < \Delta E < 0.05$ GeV for $\ell = e$ ($\ell = \mu$).

Large irreducible background contributions arise from charmonium decays $B \to K^{(*)}J/\psi$ and $B \to K^{(*)}\psi(2S)$, in which the $c\bar{c}$ state decays into two leptons. These decays have the same signature as the desired signal and are vetoed with the following requirements on $q^2 = M_{\ell^+\ell^-}$, the invariant mass of the lepton pair:

$$-0.25\ \text{GeV}/c^2 < M_{ee(\gamma)} - m_{J/\psi} < 0.08\ \text{GeV}/c^2,$$
$$-0.15\ \text{GeV}/c^2 < M_{\mu\mu} - m_{J/\psi} < 0.08\ \text{GeV}/c^2,$$
$$-0.20\ \text{GeV}/c^2 < M_{ee(\gamma)} - m_{\psi(2S)} < 0.08\ \text{GeV}/c^2 \text{ and}$$
$$-0.10\ \text{GeV}/c^2 < M_{\mu\mu} - m_{\psi(2S)} < 0.08\ \text{GeV}/c^2.$$

In the electron case, the 4-momentum of detected photons from the bremsstrahlung recovery process is added

before these requirements are applied. Di-electron background can also arise from photon conversions ($\gamma \to e^+e^-$) and π^0 Dalitz decays ($\pi^0 \to e^+e^-\gamma$). We require $M_{e(\gamma)e(\gamma)} > 0.14$ GeV/c^2. For the B meson candidates, a vertex fit is performed, which is used for background suppression. From this fit the distance between the two leptons along the beam direction $\Delta z_{\ell\ell}$ is also derived.

IV. BACKGROUND SUPPRESSION

In the selection of B candidates we face different sources of possible backgrounds. In continuum background events, e^+e^- annihilates into light quark pairs $u\bar{u}, d\bar{d}, s\bar{s}$ as well as events containing charm quarks $c\bar{c}$. These initial quark pairs however exhibit a large energy release, forming back to back jet–like structures. Combinatorial background arises from incorrect combinations of tracks in $B\bar{B}$ decays, which is the dominant source of background. Finally, a process is referred to as "peaking background" when it mimics the signal shape in $M_{\rm bc}$. For the peaking background several sources have to be taken into account: (1) irreducible background from $B \to K^*J/\psi$ and $B \to K^*\psi(2S)$ events, which passes the q^2 vetoes; (2) doubly misidentified events from $B \to K^*\pi\pi$ can occur when both pions are misidentified as muons.

To maximize signal efficiency and purity, neural networks are developed sequentially from the bottom to the top of the decay chain, transferring each time the output probability to the subsequent step so that the most effective selection requirements are applied in the last stage based on all information combined. All particle candidates are analyzed with a neural network (NeuroBayes [8]) and an output, $NB_{\rm out}$, is assigned. This output is chosen to correspond to a Bayesian probability in the range $[0, 1]$ where the value of one corresponds to signal. To transfer quality information about the primary particles in the detector to higher stage composite particles (K^* and B) the network output of the secondary particles of each candidate is included as neural network input. In this manner the classifiers for the B mesons have $NB_{\rm out}$ for both leptons and the K^* included as input. The classifiers for $e^\pm, \mu^\pm, K^\pm$ and $\pi^\pm$ are taken from the neural network based full reconstruction, widely used at Belle [9]. They use kinematic variables as inputs as well as variables derived from the particle identification system, for instance TOF and KLM information and energy loss in the CDC. For K^* selection a classifier is trained on simulated data using kinematic variables and vertex fit information. The final classification is performed with a requirement on the neural network output $NB_{\rm out}$ for the B mesons. Separate classifiers are trained for $B^0 \to K^*(892)^0\mu^+\mu^-$ and $B^0 \to K^*(892)^0e^+e^-$ using event shape variables (i.e. Fox Wolfram Moments [10]), vertex fit information and kinematic variables. The most important variables for the neural networks are ΔE, the reconstructed mass of the K^*, the product of the network outputs of all secondary particles and the distance between the two leptons along the beam direction $\Delta z_{\ell\ell}$. In case of multiple candidates per event the most probable candidate is chosen, based on the neural network output $NB_{\rm out}$. The final neural network output for signal and background events is displayed in Figure 1.

The selection requirement for the neural networks are optimized for the sensitivity of the angular analysis using pseudo experiments with simulated data, described in Section VI.

V. SIGNAL YIELDS

Signal and background yields are extracted by an unbinned extended maximum likelihood fit to the $M_{\rm bc}$ distribution of $B^0 \to K^*(892)^0\ell^+\ell^-$candidates. The signal distribution is parametrized by an empirically determined function introduced by the Crystal Ball Collaboration [11]. This so-called Crystal Ball function accounts for radiative tails in the distribution and for the calorimeter resolution. All shape parameters are determined by a fit to data in the control channel $B \to K^*J/\psi$ in the corresponding q^2 veto region and fixed in the extraction of the $B^0 \to K^*(892)^0\ell^+\ell^-$yield. The background distribution is parametrized by an empirically determined shape introduced by the ARGUS Collaboration [12] and its shape parameters are floated in the fit. The result of the fits are shown in Figure 2. In the total q^2 range there are 118 ± 12 signal candidates for $B^0 \to K^*(892)^0\mu^+\mu^-$ and 69 ± 12 for $B^0 \to K^*(892)^0e^+e^-$. For the angular analysis the number of signal events $n_{\rm sig}$ and background events $n_{\rm bkg}$ in the signal region $M_{\rm bc} > 5.27$ GeV/c^2 are obtained by a fit to $M_{\rm bc}$ in bins of q^2. The extracted yields and the definition of the bin ranges are presented in Table I. As a cross-check, the branching fractions for both modes are calculated and found to be consistent with PDG values within statistical errors.

TABLE I. Fitted yields and statistical error for signal ($n_{\rm sig}$) and background ($n_{\rm bkg}$) events in the binning of q^2 for both the combined electron and muon channel.

Bin	q^2 range in GeV$^2/c^4$	$n_{\rm sig}$	$n_{\rm bkg}$
0	$1.00 - 6.00$	49.5 ± 8.4	30.3 ± 5.5
1	$0.10 - 4.00$	30.9 ± 7.4	26.4 ± 5.1
2	$4.00 - 8.00$	49.8 ± 9.3	35.6 ± 6.0
3	$10.09 - 12.90$	39.6 ± 8.0	19.3 ± 4.4
4	$14.18 - 19.00$	56.5 ± 8.7	16.0 ± 4.0

VI. ANGULAR ANALYSIS

We perform an angular analysis of $B^0 \to K^*(892)^0\ell^+\ell^-$ including the electron and muon modes. The decay is kinematically described by three angles θ_ℓ, θ_K and ϕ and the invariant mass squared

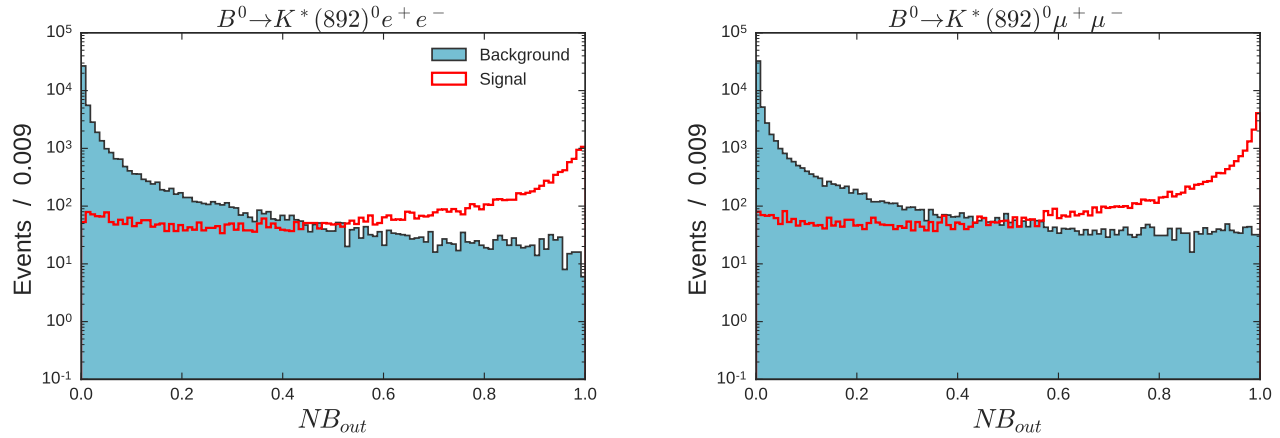

(a)$NB_{\rm out}$ for $B^0 \to K^*(892)^0 e^+ e^-$ (b)$NB_{\rm out}$ for $B^0 \to K^*(892)^0 \mu^+ \mu^-$

FIG. 1. Performance of the neural networks for the classification of $B^0 \to K^*(892)^0 \ell^+ \ell^-$. Signal MC (red line) and simulated background processes from $e^+e^- \to q\bar{q}$ ($q = u, d, s, c, b$) decays (blue filled) corresponding to two times the expected size in the Belle dataset are shown.

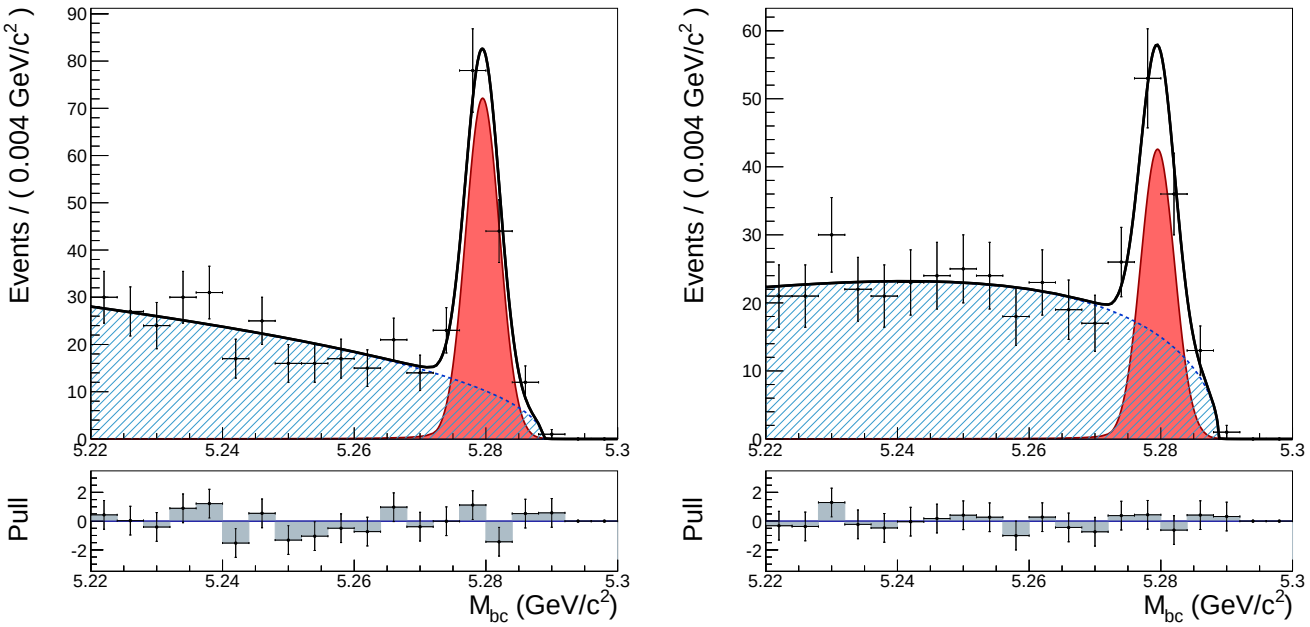

(a)$B^0 \to K^*(892)^0 \mu^+ \mu^-$ (b)$B^0 \to K^*(892)^0 e^+ e^-$

FIG. 2. Signal extraction for $B \to K^{(*)} \ell^+ \ell^-$ on the total range of q^2. Combinatorial (dashed blue), signal (red filled) and total (solid) fit distributions are superimposed on the data points.

of the lepton pair q^2. The angle θ_ℓ is defined as the angle between the direction of ℓ^+ (ℓ^-) and the opposite direction of B ($\bar{B}$) in the rest frame of the dilepton system. The angle θ_K is defined between the direction of the kaon and the opposite direction of B ($\bar{B}$) in the K^* rest frame. Finally, the angle ϕ is determined as the angle between the decay plane formed by the $\ell^+\ell^-$ system and the K^* decay plane. Definitions of the angles follow Ref. [13]. The analysis is performed in four bins of q^2 with an additional zeroth bin in the range $1.0 < q^2 < 6.0$ GeV$^2/c^4$, which is considered to be the cleanest regarding form-factor uncertainties [14]. The binning in q^2 is detailed in Table I together with the measured signal and background yields. Uncovered regions in the q^2 spectrum arise from vetoes against backgrounds of the charmonium resonances $J/\psi \to \ell^+\ell^-$ and $\psi(2S) \to \ell^+\ell^-$ and vetos against π^0 Dalitz decays and photon conversion.

The full angular distribution of $B \to K^{*0}(\to K^{\pm}\pi^{\mp})\ell^+\ell^-$ can be parametrized using definitions presented in Ref. [14] by

$$\begin{aligned}\frac{1}{\mathrm{d}\Gamma/\mathrm{d}q^2}\frac{\mathrm{d}^4\Gamma}{\mathrm{d}\cos\theta_\ell\,\mathrm{d}\cos\theta_K\,\mathrm{d}\phi\,\mathrm{d}q^2} =& \frac{9}{32\pi}\Big[\frac{3}{4}(1-F_L)\sin^2\theta_K + F_L\cos^2\theta_K \\ &+ \frac{1}{4}(1-F_L)\sin^2\theta_K\cos 2\theta_\ell \\ &- F_L\cos^2\theta_K\cos 2\theta_\ell + S_3\sin^2\theta_K\sin^2\theta_\ell\cos 2\phi \\ &+ S_4\sin 2\theta_K\sin 2\theta_\ell\cos\phi + S_5\sin 2\theta_K\sin\theta_\ell\cos\phi \\ &+ S_6\sin^2\theta_K\cos\theta_\ell + S_7\sin 2\theta_K\sin\theta_\ell\sin\phi \\ &+ S_8\sin 2\theta_K\sin 2\theta_\ell\sin\phi + S_9\sin^2\theta_K\sin^2\theta_\ell\sin 2\phi\Big], \end{aligned} \tag{3}$$

where the observables F_L and S_i are functions of q^2 only. The observables are functions of Wilson coefficients, containing information about the short-distance effects and can be affected by new physics. The observables P_i', introduced in Ref. [15], defined as

$$P'_{i=4,5,6,8} = \frac{S_{j=4,5,7,8}}{\sqrt{F_L(1-F_L)}}, \tag{4}$$

are considered to be largely free from form-factor uncertainties [16]. In total, there are eight free parameters, which can be obtained from a fit to the data. The statistics in this analysis are not sufficient to perform an eight-dimensional fit. In the following a folding technique is described, which reduces the number of fitting parameters and hence improves the convergence of the fit. The folding is applied to specific regions in the three-dimensional angular space, exploiting the symmetries of the cosine and sine functions to cancel terms in Eq. (3). As a consequence the number of free parameters in the fit is reduced without losing experimental sensitivity. This procedure is explained in more detail in Refs. [17] and [18]. With the following transformations to the dataset one can be sensitive to the observable of interest:

$$P'_4, S_4: \begin{cases} \phi \to -\phi & \text{for } \phi < 0 \\ \phi \to \pi - \phi & \text{for } \theta_\ell > \pi/2 \\ \theta_\ell \to \pi - \theta_\ell & \text{for } \theta_\ell > \pi/2, \end{cases} \tag{5}$$

$$P'_5, S_5: \begin{cases} \phi \to -\phi & \text{for } \phi < 0 \\ \theta_\ell \to \pi - \theta_\ell & \text{for } \theta_\ell > \pi/2, \end{cases} \tag{6}$$

$$P'_6, S_7: \begin{cases} \phi \to \pi - \phi & \text{for } \phi > \pi/2 \\ \phi \to -\pi - \phi & \text{for } \phi < -\pi/2 \\ \theta_\ell \to \pi - \theta_\ell & \text{for } \theta_\ell > \pi/2, \end{cases} \tag{7}$$

$$P'_8, S_8: \begin{cases} \phi \to \pi - \phi & \text{for } \phi > \pi/2 \\ \phi \to -\pi - \phi & \text{for } \phi < -\pi/2 \\ \theta_K \to \pi - \theta_K & \text{for } \theta_\ell > \pi/2 \\ \theta_\ell \to \pi - \theta_\ell & \text{for } \theta_\ell > \pi/2. \end{cases} \tag{8}$$

Each of the transformations causes all S_i terms of Eq. (3), except for S_3 and the corresponding S_i term, to vanish. The number of free parameters of each transformed decay rate is consequently reduced to three: F_L, S_3 and one of the observables $S_{4,5,7,8}$ or $P'_{4,5,6,8}$.

One can extract the transverse polarization asymmetry $A_T^{(2)}$ with the transformation: $A_T^{(2)} = 2S_3/(1-F_L)$. To parameterize the background we use smoothed template histograms. A three-dimensional PDF is constructed by multiplying the histograms of each projection of the angular variables:

$$\begin{aligned} f_{\mathrm{bkg}}^{\mathrm{hist}}(q^2, \cos\theta_\ell, \cos\theta_K, \phi) = \\ h_1(q^2, \cos\theta_\ell)\cdot h_2(q^2, \cos\theta_K)\cdot h_3(q^2, \phi). \end{aligned}$$

This method is fast and robust even if the background shape is complex. The correlation in the background sample between the observables is negligible allowing for this procedure. However, it introduces systematic deviations from the true PDF due to statistical fluctuations. To compensate for this, the histograms are smoothed with an algorithm introduced in Ref. [19], which takes into account Poisson errors for bins with a small number of entries. This method aims to optimize the pull distribution from smoothed histograms to the original histogram with statistical fluctuations by a least square minimization.

All methods are tested in toy MC studies using simulated events where each measurement is performed 10,000 times. The most important optimization is that of the neural network requirement for both $B^0 \to K^*(892)^0 e^+e^-$ and $B^0 \to K^*(892)^0\mu^+\mu^-$, which determines the signal to background ratio in the fit. The sensitivity is optimized by minimizing the total error of

P_5' in q^2 bin 2. In the toy studies this is calculated as the linear sum of the mean statistical error from the toy study e_{stat}, the systematic error from a fit bias e_{bias} and the estimated error from peaking background $\hat{e}_{peaking}$. From this procedure, the estimated sensitivity for each pair of requirements is obtained.

VII. ACCEPTANCE AND EFFICIENCY

We account for acceptance and efficiency effects in the fit by assigning weights to the data. We weight each event by the inverse of its combined efficiency, which is derived from the direct product of the efficiencies of the angular observables and q^2. The individual reconstruction efficiency for each observable x is obtained by extracting the differences between the reconstructed and generated distributions. In order to minimize statistical fluctuations in this process, the generated distribution is transformed to a flat distribution. For $x_{\rm gen}$ from generated events in the signal MC the corresponding cumulative density distribution is derived by a spline interpolation $s_{\rm gen}$ from a histogram of the cumulative density distribution of $x_{\rm gen}$. In the next step we transform the $x_{\rm rec}$ value from reconstructed signal MC events, which include reconstruction and acceptance effects, with $s_{\rm gen}$ and derive the distribution of the reconstruction efficiency. The distribution of the reconstruction efficiency follows

$$x_{\rm eff} = s_{\rm gen}(x_{\rm rec}). \tag{9}$$

The final efficiency for each observable is then fitted with a spline fit $s_{\rm eff}$ to the distribution of $x_{\rm eff}$, which fits orthogonal splines to the data so that the pull between the fit and the data-points becomes a Gaussian with width one and mean zero. Finally, the efficiency $\epsilon(x)$ for observable x is calculated from

$$\epsilon(x) = s_{\rm eff}(s_{\rm gen}(x)). \tag{10}$$

The combined efficiency $f_{\rm eff}^{\rm bin}$ is determined in each bin of q^2 and is calculated by

$$f_{\rm eff}^{\rm bin}(\cos\theta_\ell, \cos\theta_K, \phi, q^2) = \epsilon(\cos\theta_\ell) \otimes \epsilon(\cos\theta_K) \otimes \epsilon(\phi) \otimes \epsilon(q^2), \tag{11}$$

assuming that the efficiency is uncorrelated in the three-dimensional angular space, which is validated for the systematic uncertainties. The fits for the efficiencies in the q^2 range $4 < q^2 < 8$ GeV$^2/c^4$ are shown in Figure 3. In the final fit the weights are normalized, so that the sum of all weights equals the total number of events in the fit.

VIII. FIT PROCEDURE

The signal and background fractions are derived from a fit to $M_{\rm bc}$ beforehand, where the yields are listed in Table I. The $M_{\rm bc}$ variable is split into a signal (upper) and sideband (lower) region at 5.27 GeV/c^2. In the second step the shape of the background for the angular observables is estimated on the $M_{\rm bc}$ sideband. This is possible as the angular observables have shown to be uncorrelated to $M_{\rm bc}$ in the background sample.

All observables $P_{4,5,6,8}'$ are extracted from the data in the signal region using three-dimensional unbinned maximum likelihood fits in four bins of q^2 and the additional zeroth bin using the folded signal PDF, fixed background shapes and a fixed number of signal events. Each $P_{4,5,6,8}'$ is fitted with F_L and $A_T^{(2)}$. Counting also the zeroth bin, which exhibits overlap with the range of the first and second bin, 20 measurements are performed.

IX. SYSTEMATIC STUDIES

For the angular analysis sources of systematic uncertainty are considered, if they introduce an angular or q^2 dependent bias to the distributions of signal or background candidates. Systematic uncertainties are examined using pseudo-experiments with large signal yields in order to minimize statistical fluctuations and compare the nominal with a varied model. The variation between the average of two models is taken as systematic uncertainty. Observed differences between data and MC are modeled within the fit for the efficiency correction as a bias. A systematic error is derived from the difference between the results from a fit with the nominal efficiency correction and the modified correction including differences observed on data. Due to the limited number of candidates in some measurements, a fit bias is observed in some bins of the angular analysis. In 10,000 pseudo experiments on simulated data the fit for each measurement is performed and the results are compared to the simulated values. The mean of the pull distribution from the toy study is used for each measurement to determine a systematic bias on the measurement. The central values of the measurements are not corrected for the bias but the absolute value of the deviation is assigned as a systematic error. For the fit of the reconstruction efficiency function a factorization of the efficiencies in the angular observables and q^2 is assumed, which is not the case for $\cos\theta_\ell$ in the low q^2 region. The deviation in a simulated dataset with efficiency correction weights and a dataset based on generator truth is evaluated. The difference between the two fits is taken into account as a systematic uncertainty for the efficiency correction in the fit.

Peaking backgrounds are estimated for each q^2 bin using MC. In total less than six such background events are expected in the muon channel, and less than one in the electron channel. The impact of the peaking component is simulated by repeating the toy study and replacing six randomly selected events from the signal with events from the peaking background in each bin. The mean deviation of the procedure is ± 0.027 for the value of $P_{4,5,6,8}'$, which corresponds to approximately $2-5\%$

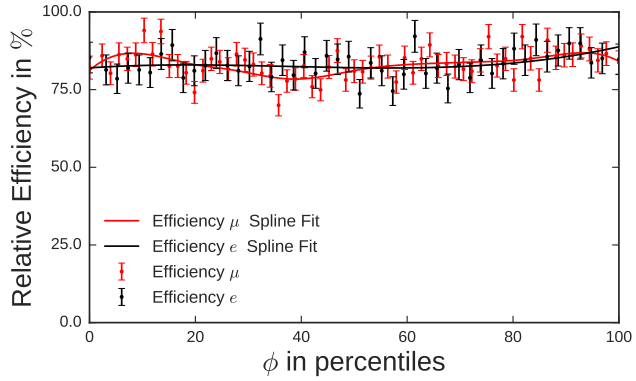

(a)Efficiency in ϕ

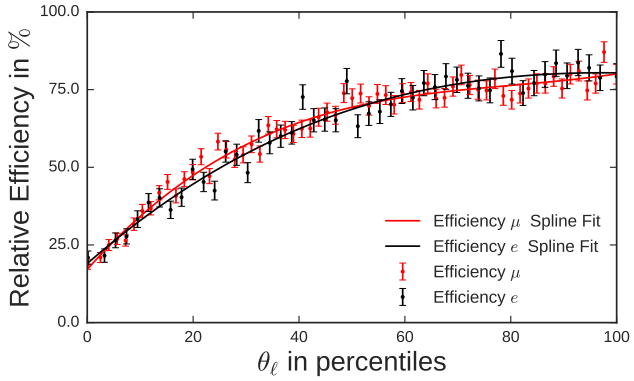

(b)Efficiency in θ_ℓ

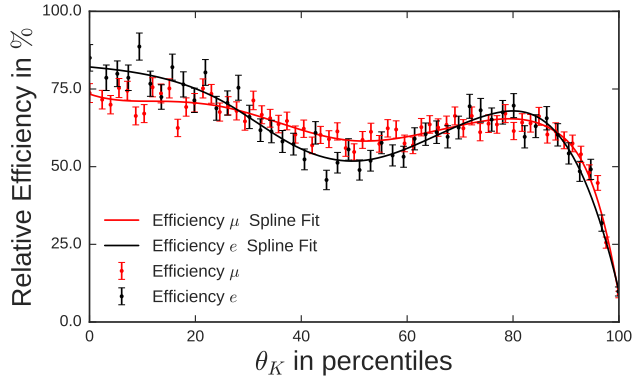

(c)Efficiency in θ_K

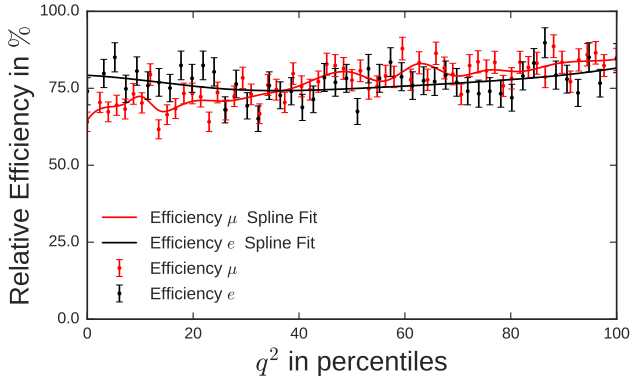

(d)Efficiency in q^2

FIG. 3. Example for the fits of the efficiencies in q^2 bin 2 . Both the efficiency fits (solid lines) for the electron (black) and muon (red) channel are superimposed over the ratio of generated and reconstructed events (data points).

of the statistical error. The signal cross-feed is calculated for the B^0 decay channels ($B^0 \to K^*(892)^0\mu^+\mu^-$, $B^0 \to K^*(892)^0e^+e^-$, $B^0 \to K^0\mu^+\mu^-$, $B^0 \to K^0e^+e^-$) and found to be insignificant. The parametrization in Eq. (3) does not include a potential S-wave contribution from $K^*(892)$ decays. The fraction F_S is searched for in our data by fitting the invariant mass of the $K\pi$ pair resulting in F_S being consistent with zero with a small uncertainty. If there is a production, detection or direct $\mathcal{CP}$ asymmetry observed, the measured $\mathcal{CP}$-symmetric parameters, must be corrected. Since the yields of B^0 and $\bar{B}^0$ events are statistically equal in the signal region of our measurement with 153 and 150 events, respectively, and the theoretical values are small for the $\mathcal{CP}$ asymmetric parameters $A_i^{(s)}$ ($\lesssim \mathcal{O}(10^{-3})$ [14]) influences of this kind are neglected. All sources of included systematics are summarized separately for P_4', P_5', P_6' and P_8' in Tables II, III, IV and V. The total systematic uncertainty is calculated as the square root of the quadratic sum of all systematic uncertainties.

TABLE II. Summary of all systematic uncertainties for P_4'.

Bin	0	1	2	3	4
Peaking Background	0.0855	0.0646	0.0366	0.0457	0.0358
Data/MC Difference	0.0109	0.0088	0.0020	0.0003	0.0047
Efficiency Correction	0.1475	0.0241	0.0599	0.0877	0.0650
Fit Bias	0.0316	0.0114	0.0007	0.0558	0.0027
Total	0.1738	0.0704	0.0702	0.1135	0.0744

TABLE III. Summary of all systematic uncertainties for P_5'.

Bin	0	1	2	3	4
Peaking Background	0.0901	0.0636	0.0078	0.0498	0.0131
Data/MC Difference	0.0112	0.0067	0.0208	0.0142	0.0029
Efficiency Correction	0.0397	0.0205	0.0098	0.0215	0.0327
Fit Bias	0.0031	0.0061	0.0430	0.0127	0.0460
Total	0.0992	0.0675	0.0494	0.0575	0.0580

TABLE IV. Summary of all systematic uncertainties for P_6'.

Bin	0	1	2	3	4
Peaking Background	0.0170	0.0513	0.0229	0.0215	0.0026
Data/MC Difference	0.1298	0.1378	0.1655	0.2201	0.2341
Efficiency Correction	0.0835	0.0432	0.0683	0.0218	0.0192
Fit Bias	0.0735	0.1189	0.0562	0.0027	0.0268
Total	0.1718	0.1939	0.1890	0.2222	0.2364

TABLE V. Summary of all systematic uncertainties for P_8'.

Bin	0	1	2	3	4
Peaking Background	0.1242	0.0161	0.0395	0.0518	0.0255
Data/MC Difference	0.1433	0.1630	0.1531	0.1955	0.2316
Efficiency Correction	0.0319	0.0824	0.0359	0.0418	0.0099
Fit Bias	0.0337	0.1033	0.0579	0.0048	0.0047
Total	0.1952	0.2105	0.1722	0.2065	0.2332

X. RESULTS

The measurements are compared with SM predictions based upon different theoretical calculations. Values from DHMV refer to the soft-form-factor method of Ref. [20], which is also used in the LHCb measurement. BSZ corresponds to using QCD form factors computed from LCSRs with K^* distribution amplitudes described in [21]. The third set of theoretical predictions is provided by the methods and authors of Refs. [22, 23] whose framework is specially tailored to the low q^2 region. It is referred to as JC. The results are listed in Table VI and are shown in Figure 5 together with available SM prediction from DHMV and LHCb measurements.

For P_5' a deviation with respect to the DHMV SM prediction is observed with a significance of 2.1σ in the q^2 range $4.0 < q^2 < 8.0$ GeV$^2/c^4$. The fit result is displayed in Figure 4 with the corresponding projections. The distance to the SM prediction from BSZ and JC corresponds to 1.72σ and 1.68σ, respectively.

The discrepancy in P_5' supports measurements by LHCb [17], where a 3.7σ deviation was observed in the region $4.30 < q^2 < 8.68$ GeV$^2/c^4$. To avoid unknown theory errors originating from the J/ψ resonance the low q^2 region is limited to $q^2 < 8.0$ GeV$^2/c^4$ in the present measurement. LHCb performed an update on the analysis [1] with three times the integrated luminosity. In the update the overall discrepancy of the differential distributions with the DHMV SM prediction was 3.4σ [1].

XI. CONCLUSION

We present results of the first angular analysis of $B^0 \to K^*(892)^0\ell^+\ell^-$in three dimensions at B factories, including both the muon and electron modes. In total 117.6 ± 12.4 signal candidates for $B^0 \to K^*(892)^0\mu^+\mu^-$ and 69.4 ± 12.0 signal events for $B^0 \to K^*(892)^0e^+e^-$ are observed. The signal yields are consistent with those expected from previous measurements. With the combined data of both channels a full angular analysis in three dimensions in five bins of q^2, the di-lepton invariant mass squared, is performed. A data transformation technique is applied to reduce the dimension of the differential decay rate from eight to three. By this means the fit is independently sensitive to observables P_4', P_5', P_6' and P_8', which are optimized regarding theoretical uncertainties from form-factors. Altogether 20 measurements are performed extracting $P_{4,5,6}'$ or P_8', the K^* longitudinal polarization F_L and the transverse polarization asymmetry $A_T^{(2)}$. The results are compared with SM predictions and overall agreement is observed. One measurement is found to deviate by 2.1σ from the predicted value into the same direction and in the same q^2 region where the LHCb collaboration reported the so-called P_5' anomaly [1, 17].

XII. ACKNOWLEDGMENTS

We thank J. Virto and J. Camalich for providing Standard Model predictions for the observables.

We thank the KEKB group for the excellent operation of the accelerator; the KEK cryogenics group for the efficient operation of the solenoid; and the KEK computer group, the National Institute of Informatics, and the PNNL/EMSL computing group for valuable computing and SINET4 network support. We acknowledge support from the Ministry of Education, Culture, Sports, Science, and Technology (MEXT) of Japan, the Japan Society for the Promotion of Science (JSPS), and the Tau-Lepton Physics Research Center of Nagoya University; the Australian Research Council; Austrian Science Fund under Grant No. P 22742-N16 and P 26794-N20; the National Natural Science Foundation of China under Contracts No. 10575109, No. 10775142, No. 10875115, No. 11175187, No. 11475187 and No. 11575017; the Chinese Academy of Science Center for Excellence in Particle Physics; the Ministry of Education, Youth and Sports of the Czech Republic under Contract No. LG14034; the Carl Zeiss Foundation, the Deutsche Forschungsgemeinschaft, the Excellence Cluster Universe, and the VolkswagenStiftung; the Department of Science and Technology of India; the Istituto Nazionale di Fisica Nucleare of Italy; the WCU program of the Ministry of Education, National Research Foundation (NRF) of Korea Grants No. 2011-0029457, No. 2012-0008143, No. 2012R1A1A2008330, No. 2013R1A1A3007772, No. 2014R1A2A2A01005286, No. 2014R1A2A2A01002734, No. 2015R1A2A2A01003280 , No. 2015H1A2A1033649; the Basic Research Lab program under NRF Grant No. KRF-2011-0020333, Center for Korean J-PARC Users, No. NRF-2013K1A3A7A06056592; the Brain Korea 21-Plus program and Radiation Science Research Institute; the Polish Ministry of Science and

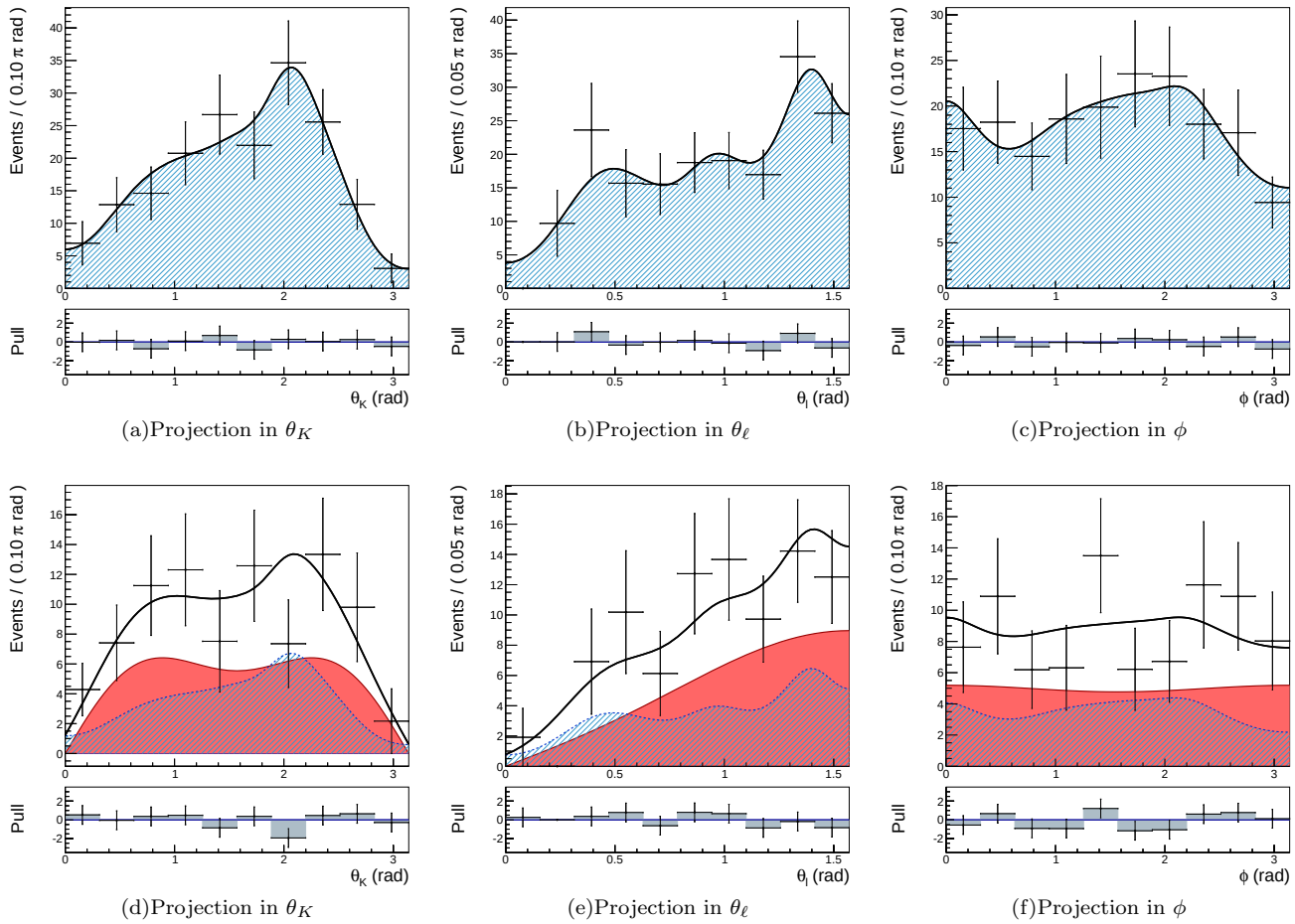

(a)Projection in θ_K (b)Projection in θ_ℓ (c)Projection in ϕ

(d)Projection in θ_K (e)Projection in θ_ℓ (f)Projection in ϕ

FIG. 4. Projections for the fit result of P_5' in bin 2. Fit to the $M_{\rm bc}$ sideband for the determination of the background shape (top) and signal region (bottom) are displayed. Combinatorial (dashed blue), signal (red filled) and total (solid) fit distributions are superimposed on the data points.

Higher Education and the National Science Center; the Ministry of Education and Science of the Russian Federation and the Russian Foundation for Basic Research; the Slovenian Research Agency; Ikerbasque, Basque Foundation for Science and the Euskal Herriko Unibertsitatea (UPV/EHU) under program UFI 11/55 (Spain); the Swiss National Science Foundation; the Ministry of Education and the Ministry of Science and Technology of Taiwan; and the U.S. Department of Energy and the National Science Foundation. This work is supported by a Grant-in-Aid from MEXT for Science Research in a Priority Area ("New Development of Flavor Physics") and from JSPS for Creative Scientific Research ("Evolution of Tau-lepton Physics").

[1] R. Aaij *et al.* (LHCb), JHEP **02**, 104 (2016), arXiv:1512.04442 [hep-ex].
[2] A. Abashian *et al.* (Belle Collaboration), Nucl. Instrum. Methods Phys. Res. Sect. A **479**, 117 (2002); also see detector section in J.Brodzicka *et al.*, Prog. Theor. Exp. Phys. **2012**, 04D001 (2012).
[3] S. Kurokawa and E. Kikutani, Nucl. Instrum. Methods Phys. Res. Sect. A **499**, 1 (2003), and other papers included in this Volume; T.Abe *et al.*, Prog. Theor. Exp. Phys. **2013**, 03A001 (2013) and references therein.
[4] D. J. Lange, Nuclear Instruments and Methods in Physics Research Section A: Accelerators, Spectrometers, Detectors and Associated Equipment **462**, 152 (2001), Proceedings of the 7th Int. Conf. on B-Physics at Hadron Machines (BEAUTY2000).
[5] T. Sjostrand, P. Eden, C. Friberg, L. Lonnblad, G. Miu, S. Mrenna, and E. Norrbin, Comput. Phys. Commun. **135**, 238 (2001), arXiv:hep-ph/0010017 [hep-ph].
[6] E. Barberio, B. van Eijk, and Z. Was, Comput. Phys. Commun. **66**, 115 (1991).
[7] R. Brun, F. Bruyant, M. Maire, A. C. McPherson, and P. Zanarini, *GEANT 3: user's guide Geant 3.10, Geant 3.11; rev. version* (CERN, Geneva, 1987).
[8] M. Feindt, ArXiv Physics e-prints (2004),

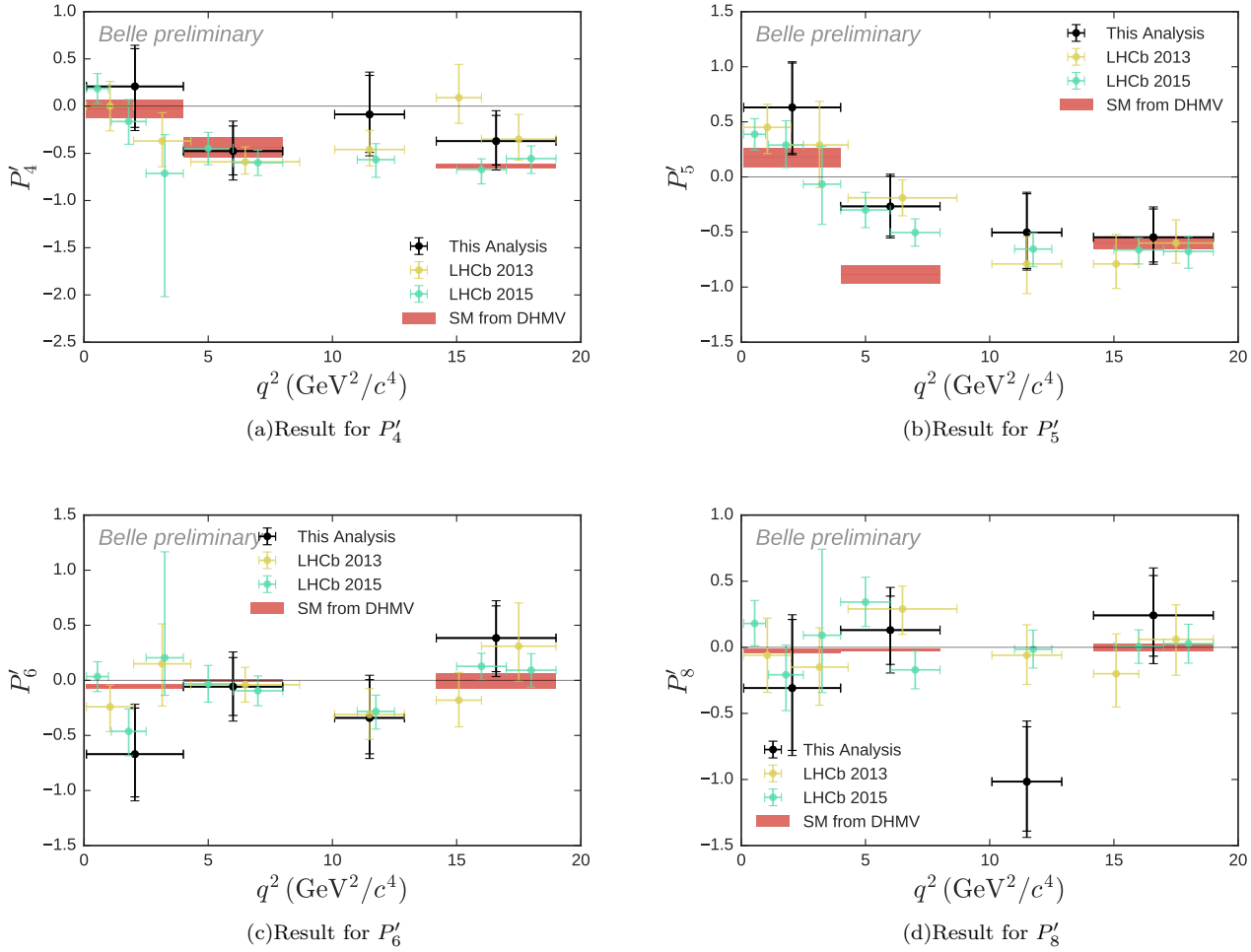

(a)Result for P_4' (b)Result for P_5'

(c)Result for P_6' (d)Result for P_8'

FIG. 5. Result for the P' observables compared to SM predictions from various sources described in Section X. Results from LHCb [1, 17] are shown for comparison.

physics/0402093.

[9] M. Feindt, F. Keller, M. Kreps, T. Kuhr, S. Neubauer, *et al.*, Nucl.Instrum.Meth. **A654**, 432 (2011), arXiv:1102.3876 [hep-ex].

[10] S. H. Lee, K. Suzuki, K. Abe, K. Abe, T. Abe, and I. . Adachi (Belle Collaboration), Phys. Rev. Lett. **91**, 261801 (2003).

[11] T. Skwarnicki, DESY-F31-86-02.

[12] H. Albrecht, Physics Letters B **340**, 217 (1994).

[13] R. Aaij *et al.* (LHCb), JHEP **08**, 131 (2013), arXiv:1304.6325.

[14] W. Altmannshofer, P. Ball, A. Bharucha, A. J. Buras, D. M. Straub, and M. Wick, JHEP **01**, 019 (2009), arXiv:0811.1214 [hep-ph].

[15] S. Descotes-Genon, J. Matias, M. Ramon, and J. Virto, JHEP **01**, 048 (2013), arXiv:1207.2753 [hep-ph].

[16] S. Descotes-Genon, T. Hurth, J. Matias, and J. Virto, JHEP **1305**, 137 (2013), arXiv:1303.5794 [hep-ph].

[17] R. Aaij *et al.* (LHCb Collaboration), Phys. Rev. Lett. **111**, 191801 (2013).

[18] M. D. Cian, *Track Reconstruction Efficiency and Analysis of $B^0 \to K^{*0}\mu^+\mu^-$ at the LHCb Experiment*, Ph.D. thesis, University of Zurich (2013).

[19] V. Blobel, *Statistische und Numerische Methoden der Datenanalyse* (1998).

[20] S. Descotes-Genon, L. Hofer, J. Matias, and J. Virto, JHEP **12**, 125 (2014), arXiv:1407.8526 [hep-ph].

[21] A. Bharucha, D. M. Straub, and R. Zwicky, (2015), arXiv:1503.05534 [hep-ph].

[22] S. Jäger and J. M. Camalich, JHEP **05**, 043 (2013), arXiv:1212.2263 [hep-ph].

[23] S. Jäger and J. M. Camalich, Phys. Rev. **D93**, 014028 (2016), arXiv:1412.3183 [hep-ph].

TABLE VI. Results of the angular analysis. The first errors of the measurement are the statistical and the second the systematic error. Observables are compared to SM predictions provided by the authors of Refs. [20, 22, 23].

q^2 in GeV$^2/c^4$	Observable	Measurement	DHMV	BSZ	JC
$[1.00, 6.00]$	P_4'	$-0.095^{+0.302}_{-0.309} \pm 0.174$	-	-	$-0.300^{+0.090}_{-0.080}$
	P_5'	$0.385^{+0.276}_{-0.285} \pm 0.099$	-	-	$-0.360^{+0.190}_{-0.170}$
	P_6'	$-0.202^{+0.278}_{-0.270} \pm 0.172$	-	-	$0.040^{+0.100}_{-0.100}$
	P_8'	$0.440^{+0.311}_{-0.320} \pm 0.195$	-	-	$0.010^{+0.020}_{-0.019}$
$[0.10, 4.00]$	P_4'	$0.208^{+0.400}_{-0.434} \pm 0.070$	-0.026 ± 0.098	-0.029 ± 0.103	$-0.010^{+0.060}_{-0.060}$
	P_5'	$0.631^{+0.403}_{-0.419} \pm 0.067$	0.175 ± 0.086	0.199 ± 0.077	$0.200^{+0.110}_{-0.110}$
	P_6'	$-0.670^{+0.419}_{-0.387} \pm 0.194$	-0.055 ± 0.018	-0.056 ± 0.018	$0.040^{+0.060}_{-0.060}$
	P_8'	$-0.309^{+0.519}_{-0.472} \pm 0.210$	-0.030 ± 0.017	-0.031 ± 0.016	$0.006^{+0.033}_{-0.033}$
$[4.00, 8.00]$	P_4'	$-0.477^{+0.266}_{-0.252} \pm 0.070$	-0.441 ± 0.106	-0.521 ± 0.087	$-0.490^{+0.070}_{-0.060}$
	P_5'	$-0.267^{+0.275}_{-0.269} \pm 0.049$	-0.881 ± 0.082	-0.770 ± 0.100	$-0.810^{+0.170}_{-0.140}$
	P_6'	$-0.057^{+0.264}_{-0.262} \pm 0.189$	-0.003 ± 0.011	-0.002 ± 0.008	$0.020^{+0.110}_{-0.110}$
	P_8'	$0.130^{+0.257}_{-0.259} \pm 0.172$	-0.022 ± 0.010	-0.020 ± 0.007	$0.007^{+0.020}_{-0.021}$
$[10.09, 12.90]$	P_4'	$-0.088^{+0.414}_{-0.402} \pm 0.114$	-	-	-
	P_5'	$-0.504^{+0.351}_{-0.327} \pm 0.057$	-	-	-
	P_6'	$-0.341^{+0.347}_{-0.326} \pm 0.222$	-	-	-
	P_8'	$-1.017^{+0.415}_{-0.374} \pm 0.207$	-	-	-
$[14.18, 19.00]$	P_4'	$-0.371^{+0.272}_{-0.252} \pm 0.074$	-0.632 ± 0.026	-0.632 ± 0.026	-
	P_5'	$-0.547^{+0.257}_{-0.225} \pm 0.058$	-0.601 ± 0.051	-0.601 ± 0.051	-
	P_6'	$0.384^{+0.292}_{-0.306} \pm 0.236$	-0.004 ± 0.069	-0.004 ± 0.069	-
	P_8'	$0.242^{+0.301}_{-0.309} \pm 0.233$	-0.001 ± 0.028	-0.001 ± 0.028	-